



# New insight of the photocatalytic behaviors of graphitic carbon nitrides for hydrogen evolution and their associations with grain size, porosity, and photophysical properties

Junghoon Oh<sup>a</sup>, Jang Mee Lee<sup>b</sup>, Youngjun Yoo<sup>c</sup>, Jeongho Kim<sup>c</sup>, Seong-Ju Hwang<sup>b</sup>, Sungjin Park<sup>a,\*</sup>

<sup>a</sup> Department of Chemistry and Chemical Engineering, WCSL (World Class Smart Lab) Green Energy Battery Lab., Inha University, 100 Inha-ro, Nam-gu, Incheon, 22212, Republic of Korea

<sup>b</sup> Department of Chemistry and Nanoscience, College of Natural Sciences, Ewha Womans University, Seoul, 03760, Republic of Korea

<sup>c</sup> Department of Chemistry and Chemical Engineering, Inha University, 100 Inha-ro, Nam-gu, Incheon, 22212, Republic of Korea



## ARTICLE INFO

### Article history:

Received 19 April 2017

Received in revised form 14 June 2017

Accepted 21 June 2017

Available online 23 June 2017

### Keywords:

Graphitic carbon nitride

Photocatalysts

Hydrogen evolution reaction

Photophysical properties

Grain size

## ABSTRACT

The development of efficient catalysts for hydrogen evolution reaction (HER) presents a huge technical challenge. Graphitic carbon nitride ( $\text{g-C}_3\text{N}_4$ ) is a promising metal-free, low cost, environment-friendly photocatalyst for HER that is driven by visible light. In this work, the authors provide new insight into the photocatalytic natures of  $\text{g-C}_3\text{N}_4$  materials and their dependences on grain size, porosity, chemical structure, and photophysical properties. Three different precursors (urea, melamine, and dicyandiamide) and two gas atmospheres (air or  $\text{N}_2$ ) are used to produce various  $\text{g-C}_3\text{N}_4$  materials. The use of urea and air leads to the formation of small grain  $\text{C}_3\text{N}_4$  networks and porous structures with large surface areas. HER catalytic activity is promoted by large surface areas and the presence of terminal amine groups, and generation of small-sized Pt nanoparticle co-catalysts with narrow size distribution on the surface of  $\text{g-C}_3\text{N}_4$ . For samples with similar surface areas, band gaps and lifetimes of photogenerated charge carriers critically determine photocatalytic activities. By examining combinations of the above-mentioned factors, urea driven  $\text{g-C}_3\text{N}_4$  produced in a  $\text{N}_2$  atmosphere is found to exhibit the best photocatalytic activity (up to  $130 \mu\text{mol h}^{-1} \text{ g}^{-1}$ ).

© 2017 Elsevier B.V. All rights reserved.

## 1. Introduction

Hydrogen evolution reaction (HER) is essential for water-splitting in various renewable and environment-friendly energy storage systems and requires efficient catalysts to overcome the activation energy required [1–5]. Reports on the electrochemical photolysis of water using  $\text{TiO}_2$  particles led to the developments of various semiconducting materials [1], such as,  $\text{MoS}_2$  [6–9],  $\text{MoSe}_2$  [10],  $\text{WS}_2$  [11,12], and  $\text{CoSe}_2$  [13] and carbon-based nanomaterial [13–16] hybrids of these with excellent HER photocatalytic performances. Specifically, visible light-active photocatalysts can be energetically favorable because visible light constitutes ~40% of solar photons [17,18]. However, the development of metal-free, low-cost, environment-friendly catalysts remains a considerable challenge.

Carbon nitride ( $\text{C}_3\text{N}_4$ )-based materials have generated research interest as possible efficient and metal-free photocatalysts for HER

[3,4,19–22]. Graphitic  $\text{C}_3\text{N}_4$  ( $\text{g-C}_3\text{N}_4$ ), which is composed of triazine or tri-*s*-triazine building units, is the most stable type of  $\text{C}_3\text{N}_4$ -based materials. They have been often reported to have excellent performances when used as photocatalysts [3,4,19–22], bioimaging probes [23,24], and optical sensors [25] due to a band gap of ~2.7 eV, which is suitable for use with visible light, numerous nitrogen sites, and their porous structures. Wang et al. demonstrated a possible application of  $\text{g-C}_3\text{N}_4$  as a metal-free photocatalyst for HER based on experimental and theoretical investigations [20]. In this previous study,  $\text{g-C}_3\text{N}_4$  was produced by thermal condensation of a cyanamide precursor and showed good catalytic activity for HER under visible light. Subsequently, tuning of the band gap by doping with heteroatoms [26,27] and increasing surface areas using template-assisted processes indicated the potential use of  $\text{g-C}_3\text{N}_4$  based materials as efficient catalysts [28,29].

Recently, the control of porosity and morphology of  $\text{g-C}_3\text{N}_4$  without the use of templates has attracted attention as a means of making materials in a cost-effective, predictable way. It has been shown that adjustments of temperature and/or time of polycondensation can be used to control structural and catalytic properties. While polymeric  $\text{C}_3\text{N}_4$  is typically produced at 550 °C, Lau et al.

\* Corresponding author.

E-mail address: [sungjinpark@inha.ac.kr](mailto:sungjinpark@inha.ac.kr) (S. Park).

reported that heat treatment of melamine at 450 °C for long time can afford melem oligomer containing increased active sites, and the materials produced showed enhanced HER photocatalytic performances [4]. Kang et al. found that sequential thermal treatment of dicyandiamide at 500 °C and 620 °C produced amorphous C<sub>3</sub>N<sub>4</sub>, which has a wider absorption range for visible light [22]. Furthermore, post-heat treatment (at 580 °C) of g-C<sub>3</sub>N<sub>4</sub> powder produced by the thermal treatment of dicyandiamide at 510 °C, broke hydrogen bonds between C<sub>3</sub>N<sub>4</sub> domains in the g-C<sub>3</sub>N<sub>4</sub> network, and resulted in the production of porous g-C<sub>3</sub>N<sub>4</sub> materials containing more active sites and significantly greater photocatalytic activity [3]. In addition, several workers have reported the use of urea as precursor leads to the production of porous C<sub>3</sub>N<sub>4</sub> materials with excellent catalytic performances [30–34].

However, the dependencies of the morphological and structural characteristics of C<sub>3</sub>N<sub>4</sub>-based materials on synthetic approaches (precursor type, temperature, time, and the gaseous environment) preclude detailed understanding of their photocatalytic natures. In the present study, we produced and characterized a series of g-C<sub>3</sub>N<sub>4</sub> materials from various precursors in different gaseous environments to explore dependences of the photocatalytic natures of g-C<sub>3</sub>N<sub>4</sub> materials on grain size, porosity, chemical structure, optical and photophysical properties, and size distribution of Pt nanoparticles as co-catalysts.

## 2. Experimental

### 2.1. Preparation of graphitic carbon nitrides (g-C<sub>3</sub>N<sub>4</sub>s) in air (CN-A)

Urea (99%), dicyandiamide (99%), and melamine (99%) powders were purchased from Sigma-Aldrich. Each precursor (2, 10, and 10 g for urea, dicyandiamide, and melamine, respectively) was loaded into an alumina crucible, which was then placed in the center of a quartz tube. The tube was heated to temperatures near the boiling point of each precursor (150, 350, and 250 °C for urea, melamine, and dicyandiamide, respectively) at a rate of 3 °C/min and then held at these temperatures for 1 h under an air flow in a muffle furnace. The temperature was then elevated to 550 °C at 3 °C/min and held for 2 h (air flow was maintained). The prepared g-C<sub>3</sub>N<sub>4</sub>s were denoted as U-CN-A, M-CN-A, and D-CN-A (where U, M, and D represent urea, melamine, and dicyandiamide, respectively, and A represents air). The quartz tube was then cooled to room temperature, to afford pale yellow powders (72 mg for U-CN-A, 1.3 g for M-CN-A, and 3.2 g for D-CN-A).

### 2.2. Preparation of graphitic carbon nitrides in N<sub>2</sub> (CN-N)

All processes were the same as described above except that N<sub>2</sub> (99.9%) was used instead of air. Before starting experiments, the quartz tube containing precursors was vacuum degassed and filled with N<sub>2</sub>. Final g-C<sub>3</sub>N<sub>4</sub> products were obtained as pale yellow powders (92 mg for U-CN-N, 3.7 g for M-CN-N, and 5.3 g for D-CN-N, N represents N<sub>2</sub>). The g-C<sub>3</sub>N<sub>4</sub>s obtained were used without further purification.

### 2.3. The photocatalytic activities of the materials produced

Photocatalytic activities were investigated in a top-irradiated vessel connected to a gas circulation system. As synthesized g-C<sub>3</sub>N<sub>4</sub> powder (100 mg) containing 3 wt% of Pt co-catalyst was suspended in 100 ml of an aqueous solution containing 10 vol% triethanolamine as a sacrificial agent. The mixture was then irradiated using a 300 W Xe lamp (Newport Stratford Inc.) fitted with an optical cut-off filter ( $\lambda > 420$  nm). Amounts of H<sub>2</sub> evolved were determined with gas chromatography (Shimadzu GC-2014).

### 2.4. Band position calculation

Band positions of g-C<sub>3</sub>N<sub>4</sub>s were determined using CV curves obtained using a potentiostat IVIUMSTAT (Ivium Technologies, USA) and a conventional three-electrode cell. A Pt mesh and Ag/AgCl electrode (+0.198 V vs NHE) were used as a counter and reference electrodes, respectively, and 0.5 M Na<sub>2</sub>SO<sub>4</sub> was used as electrolyte. The working electrodes were prepared by doctor blading a material with the help of Nafion binder on a FTO substrate.

### 2.5. Characterization

X-Ray photoelectron spectroscopy (XPS) was performed using an angle-resolved X-ray photoelectron MXR1 Gun spectrometer operated at 400 μm and 15 kV (Theta probe, Thermo Fisher Scientific, UK); the analysis was performed with sample attached by copper tape and binding energies were determined versus the N 1s peak at 398.8 eV. Peak fitting was conducted using a mixed Gaussian-Lorentz product function after subtraction of a linear background from the spectra. Full width half maximum (FWHM) parameter with 1.35 eV was used to adjust peak fitting.

Elemental analysis was conducted using a FLASH EA1112 instrument (Thermo Electron, Italy) for C, N, H, and a Vario Micro Cube (Elementar Analysensysteme GmbH, Germany) for oxygen. X-ray diffraction (XRD) patterns were obtained using a DMAX-2500 unit (Rigaku, Tokyo, Japan). Photoluminescence (PL) spectra were obtained using a spectrograph ( $f=0.5$  m, Spectrograph 500i, Acton Research Co., USA) equipped with an intensified CCD (PI-MAX3, Princeton Instruments, IRY1024, USA) and He-Cd 325 nm laser. Fourier-transform infrared (FT-IR) spectra of samples in KBr pellets were obtained using 64 scans of an FT-IR vacuum spectrometer (VERTEX 80 V, Bruker, Germany). Nitrogen adsorption-desorption measurements were carried in a Micromeritics ASAP 2010 device at 77.3 K. The surface area and pore diameter were obtained using Brunauer–Emmett–Teller (BET) and Barrett–Joyner–Halenda (BJH) methods, respectively. Transmission electron microscopy (TEM) images, selected area electron diffraction (SAED), and energy-dispersive X-ray spectroscopy (EDS) were obtained using a JEOL JEM2100F instrument (JEOL Co. Ltd., Japan) at 200 kV equipped with an EDAX analyzer (INCA X-stream Oxford Instruments, UK). Samples for TEM analysis were prepared by drying a droplet of a mixture including g-C<sub>3</sub>N<sub>4</sub> powder in water on a carbon-coated copper grid (LC300-Cu, Electron Microscopy Sciences). Scanning electron microscopy (SEM) images of Pt-coated samples were obtained using a high resolution field emission scanning electron microscope (SU 8010, Hitachi, Tokyo) at an accelerating voltage of 15 kV. Thermogravimetric analysis (TGA) measurements (SDT Q600, TA Instruments) were performed at a heating rate of 5 °C/min from 30 to 800 °C in a N<sub>2</sub> environment. UV-vis diffuse reflectance absorption spectra were obtained using a UV-2600 (Shimadzu, Japan) equipped with an ISR-2600 Plus integrating sphere attachment. Time-resolved photoluminescence (TR-PL) was measured using a time-correlated single photon counting spectrometer (FluoTime 200, PicoQuant) at room temperature. All samples prepared with pellet type were excited using 100 ps laser pulses of 390 nm center wavelength and emission was performed at 500 nm. The nominal temporal resolution of TR-PL measurements was ~190 ps.

## 3. Results and discussion

In this work, we prepared six g-C<sub>3</sub>N<sub>4</sub> samples by solid-state high-temperature polycondensation using three common monomers (melamine, dicyandiamide, and urea) in two gas environments (air or N<sub>2</sub>). We first measured the HER photocatalytic performances of all g-C<sub>3</sub>N<sub>4</sub> materials under visible light.

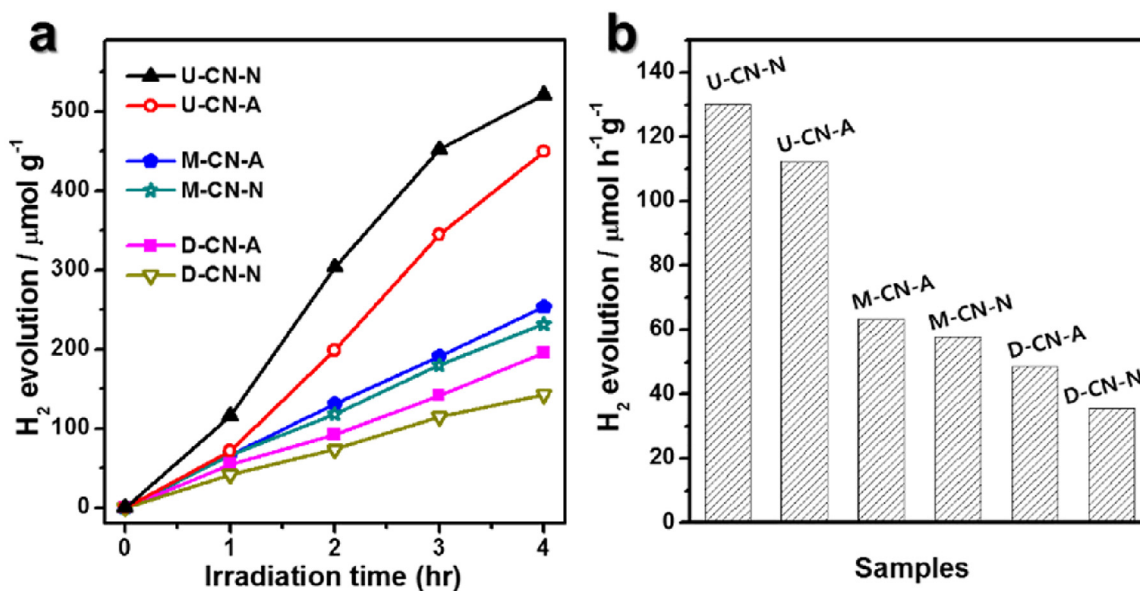


**Fig. 1.** Photocatalytic hydrogen evolution activities of  $\text{g-C}_3\text{N}_4$  samples. a) Graphs of amounts of  $\text{H}_2$  produced as a function of irradiation time to visible light ( $\lambda > 420 \text{ nm}$ ). b) Photocatalytic hydrogen evolution rates averaged over 4 h using graph a).

**Table 1**  
Properties of the six  $\text{g-C}_3\text{N}_4$  samples.

Gas	Melamine		Dicyandiamide		Urea	
	Air	$\text{N}_2$	Air	$\text{N}_2$	Air	$\text{N}_2$
sample name	M-CN-A	M-CN-N	D-CN-A	D-CN-N	U-CN-A	U-CN-N
HER catalytic activity ( $\mu\text{mol h}^{-1} \text{g}^{-1}$ )	63	58	49	36	112	130
Surface area ( $\text{m}^2/\text{g}$ )	26	12	16	6	68	68
Normalized activity (catalytic activity/surface area)	2.44	4.94	2.96	5.65	1.65	1.92
Band gap energy (eV)	2.65	2.65	2.69	2.69	2.86	2.78
Lifetime of photoexcited electrons (ns)	6.0	7.0	7.9	10.2	6.3	7.6
N-(C)3/NHx ratio	1.45	1.55	1.46	1.58	1.41	1.42
Pore diameter ( $\text{\AA}$ )	36	27	35	22	37	38

As shown in Fig. 1 and Table 1, all materials (see experimental section for sample naming) showed good photocatalytic activity and amounts of  $\text{H}_2$  evolution gradually increased up to 4 hr. Of the samples, the U-CN-N showed the highest activity of  $130 \mu\text{mol h}^{-1} \text{g}^{-1}$ , which is comparable to other efficient  $\text{C}_3\text{N}_4$ -based materials (Table S1) [21,27,28,30,35–40]. The activity of U-CN-A was slightly lower than that of U-CN-N, but was still significantly higher than those of M-CN and D-CN materials.

When we compared the catalytic activities of materials produced from the same precursors, the use of  $\text{N}_2$  was found to produce more active catalysts in the urea system but less active ones in melamine and dicyandiamide systems. The reason for this phenomenon is discussed below. Morphological characteristics of the six  $\text{C}_3\text{N}_4$  materials produced were investigated by SEM (Fig. 2). Samples produced in  $\text{N}_2$  had relatively smooth surfaces (Fig. 2a–c), whereas samples (Fig. 2d–f) produced in air had porous structures. The porosities of urea-produced  $\text{C}_3\text{N}_4$  samples were more obvious than those of melamine- or dicyandiamide-produced samples.

The same morphological trend was also observed by TEM (Fig. 3). U-CN-N and U-CN-A had highly porous structures (Fig. 3a and d) regardless of the gas used. M-CN-N and D-CN-N (Fig. 3b and c) did not exhibit porous structures, while the structures of M-CN-A and D-CN-A were slightly porous (Fig. 3e and f).

The BET surface areas of urea-produced samples (U-CN-A and U-CN-N) were  $\sim 68 \text{ m}^2/\text{g}$ , and comparable to the largest values reported for  $\text{C}_3\text{N}_4$  materials (Table S2) [21,27,30,31,35–37,40–48], and larger than those of M-CN and D-CN. While U-CN-A and U-CN-N had almost identical surface areas, the surface areas

of air-treated D-/M-CN samples were larger than those of  $\text{N}_2$ -treated D-/M-CN samples. Pore diameter, which was obtained from Barrett–Joyner–Halenda (BJH) pore size distribution curves, showed almost identical trend to the BET surface area (Fig. S1 and Table 1). These data suggested air-treatment tends to favor a more porous structure and a higher surface area than  $\text{N}_2$ -treatment. These data suggested air-treatment tends to favor a more porous structure and a higher surface area than  $\text{N}_2$ -treatment.

All X-ray diffraction (XRD) patterns (Fig. 4a) exhibited two peaks at  $27.3^\circ$  and  $13.1^\circ$ , corresponding to the inter-planar distance between  $\text{C}_3\text{N}_4$  layers and the in-planar structural packing motif of tri-*s*-triazine, respectively, which indicated that our materials contain a heptazine ring-based  $\text{C}_3\text{N}_4$  network [3,19,20,22]. Peaks were sharp for M-/D-CN samples, but relatively broad for U-CN samples. In particular, peak intensity at  $13^\circ$  in the patterns of U-CN samples was significantly reduced, implying that the in-plane structure was disrupted [3,22].

These microscopic and structural analyses indicated that types of precursors and the gases used importantly determined the morphologies of the  $\text{g-C}_3\text{N}_4$  materials produced. Because urea contains oxygen-containing species,  $\text{CO}_2$  and  $\text{H}_2\text{O}$  are generated during polycondensation of urea. It is accepted that the gas molecules adsorbed on the reaction intermediates prevent full condensation, and thus, hamper long-range in-plane structural packing, which would explain the low crystallinity and porous nature of U-CN materials. Furthermore, U-CN-N and U-CN-A materials had similar porosities and crystallinities regardless of the gaseous environments used. On the other hand, melamine and dicyandiamide have

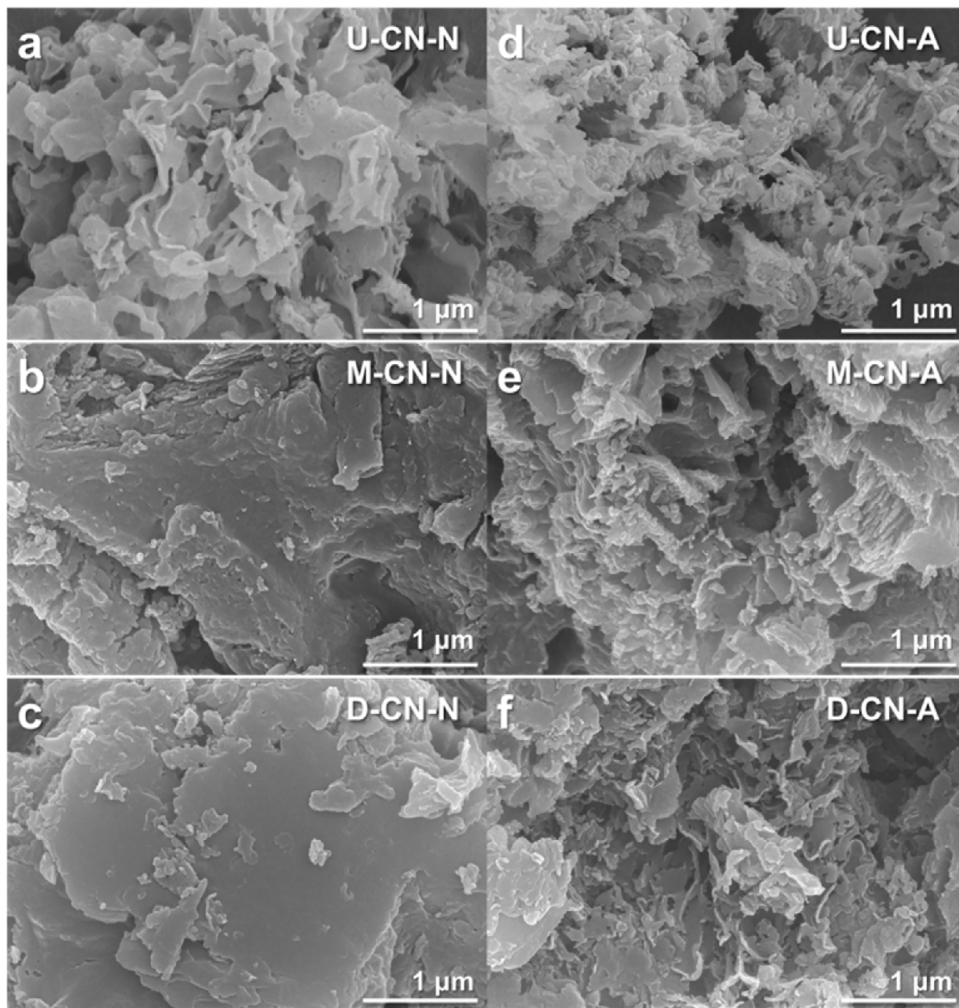


**Fig. 2.** SEM images of g-C<sub>3</sub>N<sub>4</sub> samples. a) urea-, b) melamine-, and c) dicyandiamide-derived g-C<sub>3</sub>N<sub>4</sub> prepared under N<sub>2</sub>, d) urea-, e) melamine-, and f) dicyandiamide-derived g-C<sub>3</sub>N<sub>4</sub> prepared in an air environment.

no oxygen atoms, and do not generate CO<sub>2</sub> or H<sub>2</sub>O during polycondensation, and thus, the gaseous environment becomes a dominant factor to determine the structural properties of resulting materials.

We further analyzed the chemical structures of the C<sub>3</sub>N<sub>4</sub> materials produced. In Fourier-transform infrared (FT-IR) spectra of all samples (Fig. 4b), characteristic peaks for heptazine-derived repeating units were observed at 1640, 1569, 1462, and 1412 cm<sup>-1</sup> and a triazine ring peak was observed at 810 cm<sup>-1</sup> [3,19,36]. Peaks at 1321 and 1243 cm<sup>-1</sup> were attributed to completely condensed C—N moieties and partially condensed C—NH moieties, respectively [23,41]. The spectra of U-CN samples showed a large peak at ~3420 cm<sup>-1</sup>, corresponding to —NH<sub>x</sub> stretching mode (Fig. S2) [49,50], which was also observed as a small shoulder in the spectra of M-/D-CN samples.

X-ray photoelectron spectroscopy (XPS) C 1s spectra of all samples exhibited a major peak at 288.2 eV, corresponding to the N=C—N moieties of triazine building units (Fig. S3) [3,4,19,22]. Deconvoluted XPS N 1s spectra showed a typical peak pattern for g-C<sub>3</sub>N<sub>4</sub> with peaks at 398.8, 400.1, and 401.4 eV, corresponding to C=N—C groups, tertiary N atoms, and amino functional groups, respectively (Fig. 5) [3,4,19,22]. Interesting trend was observed when N-associated species were quantified using deconvoluted N 1s spectra. While partially polymerized polymeric melon or melem oligomer contains terminal amine groups, fully condensed C<sub>3</sub>N<sub>4</sub> materials did not contain amine groups but rather tertiary N species

(N-(C)<sub>3</sub>). Consequently, a high N-(C)<sub>3</sub>/NH<sub>x</sub> ratio indicates the presence of a more condensed C<sub>3</sub>N<sub>4</sub> network.

As shown in Fig. 6, the use of air generated C<sub>3</sub>N<sub>4</sub> networks containing more NH<sub>x</sub> groups than N<sub>2</sub>, which concurs with our FT-IR results. In the case of the urea sourced material, both U-CN-A and U-CN-N samples had similar N-(C)<sub>3</sub>/NH<sub>x</sub> ratios, and these were significantly smaller than those of M-CN and D-CN samples. For melamine- and dicyandiamide-derived materials, the N-(C)<sub>3</sub>/NH<sub>x</sub> ratios of M-CN-A and D-CN-A were smaller than those of M-CN-N and D-CN-N, respectively.

Because amine groups are located at the edges of C<sub>3</sub>N<sub>4</sub> layers, a smaller N-(C)<sub>3</sub>/NH<sub>x</sub> ratio indicates more edge structures, and in turn, the presence of small grain size C<sub>3</sub>N<sub>4</sub>. HER processes convert H<sup>+</sup> to H<sub>2</sub>, and thus, efficient active species would have good H<sup>+</sup> affinity [2,20,28,51]. N atoms of terminal NH<sub>x</sub> groups have sp<sup>3</sup> hybrid orbitals, whereas the N atoms of N-(C)<sub>3</sub> groups in C<sub>3</sub>N<sub>4</sub> networks have sp<sup>2</sup> orbitals. The lone pair electrons of the former have stronger Lewis basicity than those of the latter, and thus, the formation of an adduct between H<sup>+</sup> and NH<sub>x</sub> is more favorable than the formation of one between H<sup>+</sup> and N-(C)<sub>3</sub>, which suggests NH<sub>x</sub> groups on C<sub>3</sub>N<sub>4</sub>-based materials are likely to improve photocatalytic activity. Indeed, urea-based materials had better photocatalytic activities than melamine or dicyandiamide-based materials. Crystallite size of all six g-C<sub>3</sub>N<sub>4</sub> materials was calculated using XRD data with Scherrer equation (Table S3) [52]. Crystallite size is usually considered to be smaller than or the same as

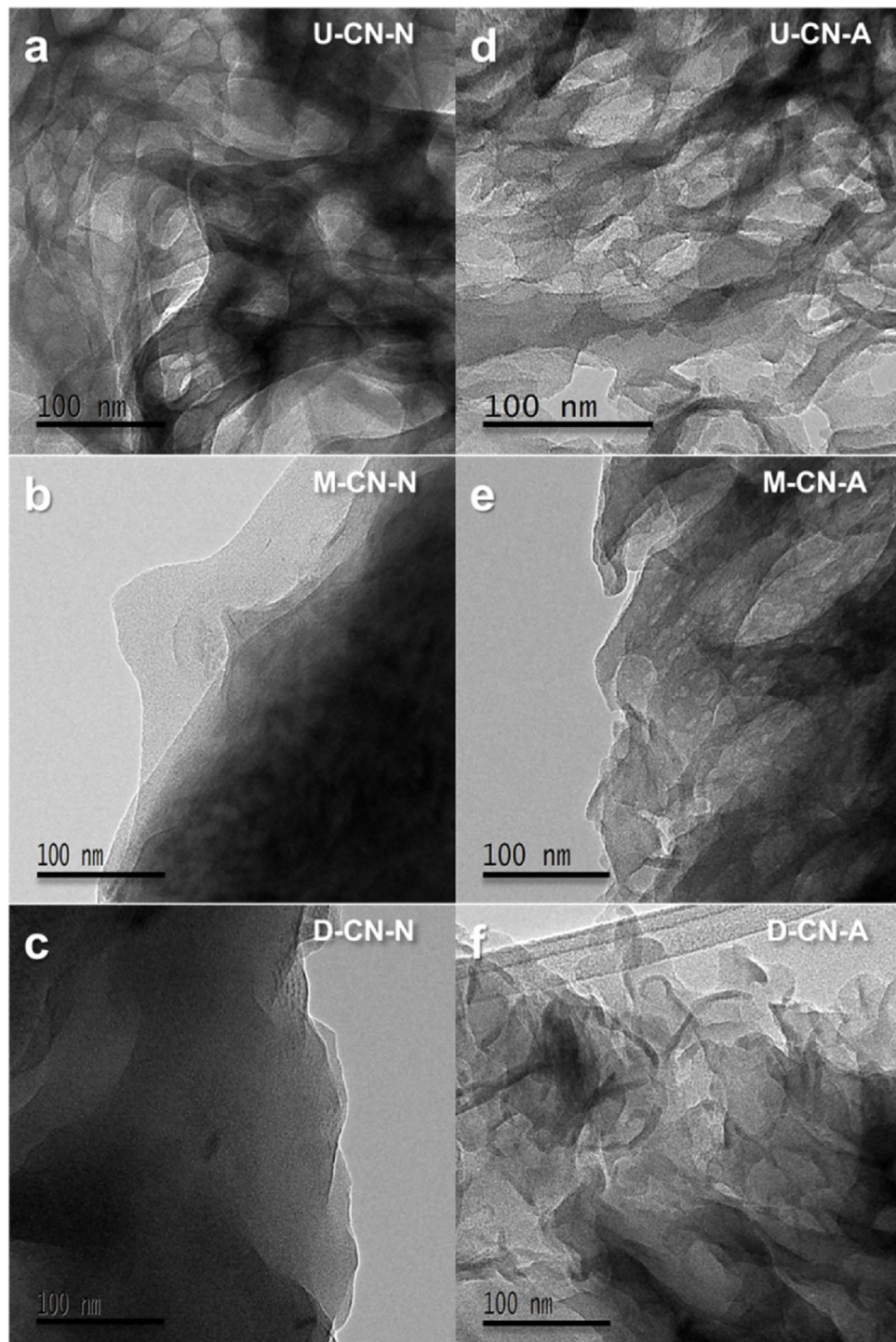


**Fig. 3.** TEM images of the six  $\text{g-C}_3\text{N}_4$  samples. a) urea-, b) melamine-, and c) dicyandiamide-derived  $\text{g-C}_3\text{N}_4$  prepared in  $\text{N}_2$  gas. d) urea-, e) melamine-, and f) dicyandiamide-derived  $\text{g-C}_3\text{N}_4$  prepared in air.

grain size. Those of U-CN samples were smaller than those of M- and D-CN samples, which is identical to trend of grain size determined by  $\text{N}-(\text{C})_3/\text{NH}_x$  ratio. This also supports the prior photocatalytic activity of urea-based materials relative to melamine or dicyandiamide-based materials.

Photophysical properties are one of the most important characteristics to understand catalytic nature of photocatalysts. The absorption spectra of all powder samples showed similar features with broad, strong absorption at 250–500 nm (Fig. S4). Band gaps of the materials were calculated from the absorption spectra using

the Kubelka-Munk function (Fig. S5) and were determined to be 2.65 eV, 2.69 eV, 2.78 eV and 2.86 eV for M-CN-A/M-CN-N, D-CN-A/D-CN-N, U-CN-N, and U-CN-A, respectively [53]. These values are close to the previously reported band gap values of  $\text{g-C}_3\text{N}_4$  materials (Table S2). These results show that all six materials absorb visible light.

As shown in Fig. 7, the conduction bands of the six materials are located at lower energies than the hydrogen evolution potential (0 V vs. the NHE), which means they possess a band structure suitable for HER [2,20]. Generally, M- and D-CN samples have smaller

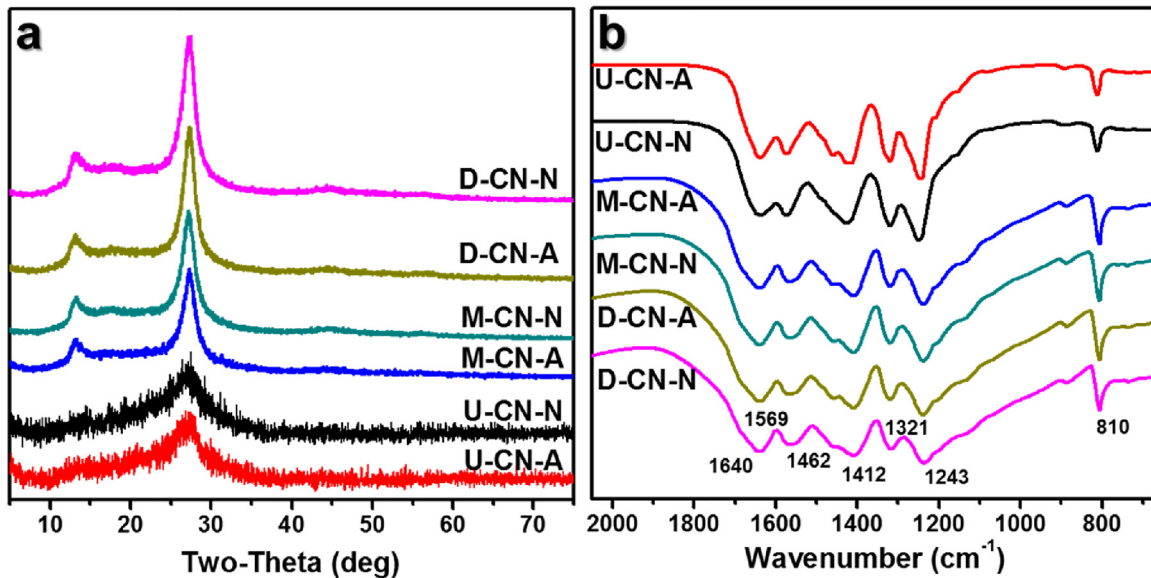


**Fig. 4.** Chemical characterizations of the as-prepared  $\text{g-C}_3\text{N}_4$  samples: a) XRD patterns and b) FT-IR spectra at selected region.

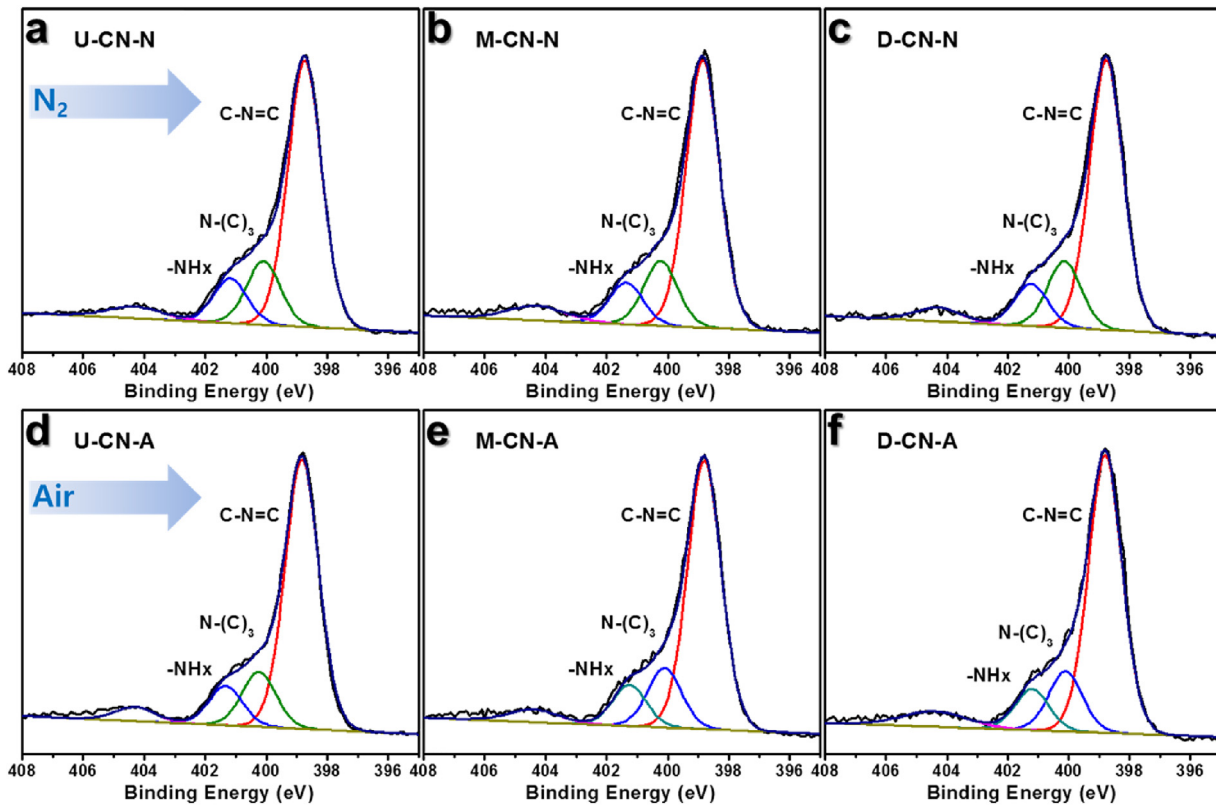


**Fig. 5.** Deconvoluted XPS N 1s spectra of the  $\text{g-C}_3\text{N}_4$  samples. a) U-CN-N, b) M-CN-N, c) D-CN-N, d) U-CN-A, e) M-CN-A, and f) D-CN-A.

band gaps than U-CN samples, which can be explained by differences in degree of condensation.

As mentioned above, M- and D-CN samples have higher degrees of condensation than U-CN samples, which results in longer conjugation of  $\text{C}_3\text{N}_4$  network, and thus, smaller band gaps as indicated by red-shift of the absorption edge [54]. Among the two urea-based samples, U-CN-N (2.78 eV) was found to have a smaller band gap than U-CN-A (2.86 eV), suggesting that U-CN-N is able to use visible light for photocatalysis better than U-CN-A.

For further understanding of the photophysical properties of photo-excited charge carriers in CN materials, we measured photoluminescence (PL) spectra and time-resolved PL decay. All the PL spectra of the six samples show a strong emission peak at  $\sim 500$  nm due to band-to-band recombination of photogenerated charge carriers (Fig. S6) [3,55]. Fig. S7 shows the time-resolved PL signals of the CN materials measured at 500 nm, and Table 2 shows fit parameters for multi-exponential fits of PL decay. Notably, for all three precursor systems, CN materials produced in air show slightly faster PL decay than those prepared in  $\text{N}_2$  (Tables 1 and 2). PL decay is

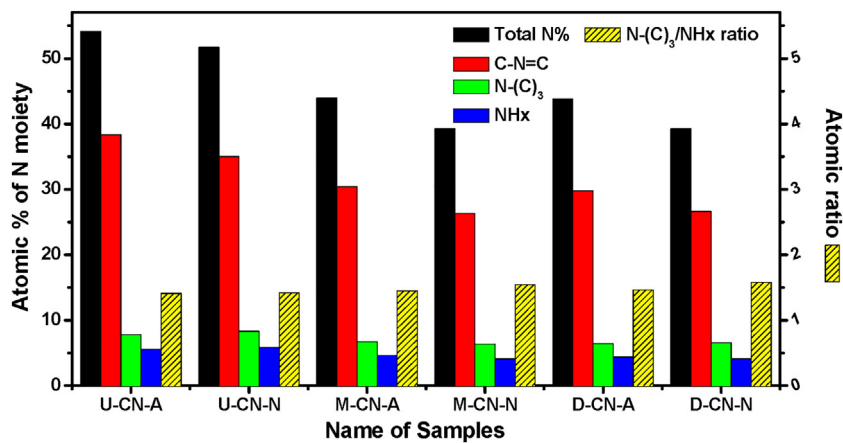


**Fig. 6.** Quantitative comparisons of the nitrogen compositions of the six g-C<sub>3</sub>N<sub>4</sub> samples as determined using deconvoluted N 1s XPS spectra.

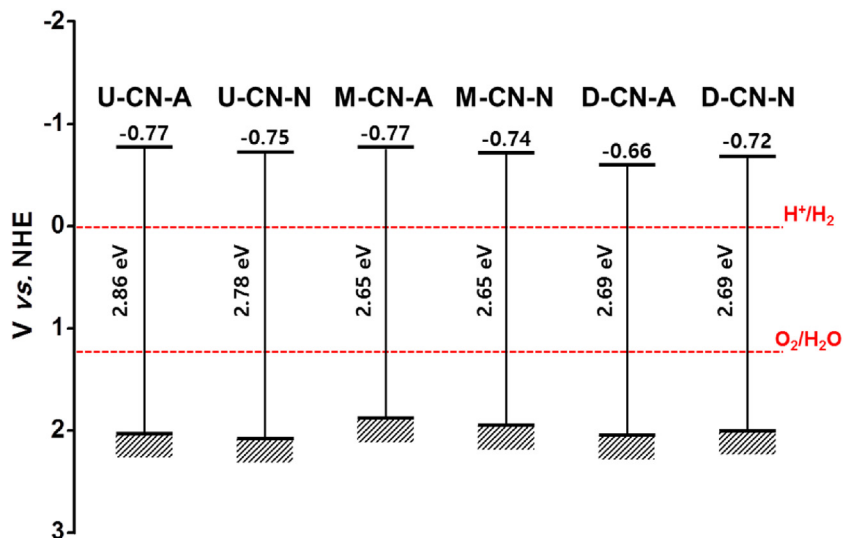


**Fig. 7.** Energy diagram showing the positions of valence and conduction bands of the six g-C<sub>3</sub>N<sub>4</sub> samples.

**Table 2**

Photoluminescence decay time ( $\tau$ ) and the fractional amplitudes (f) of the six g-C<sub>3</sub>N<sub>4</sub> samples.

Sample	Decay time (ns)			Fractional amplitude (%)			Average lifetime ( $\tau_{av.}$ , ns) <sup>a</sup>
	$\tau_1$	$\tau_2$	$\tau_3$	f <sub>1</sub>	f <sub>2</sub>	f <sub>3</sub>	
U-CN-A	11.68	2.20	0.56	8.28	39.27	52.44	6.29
U-CN-N	12.54	2.19	0.49	10.19	38.61	51.21	7.58
M-CN-A	11.83	1.83	0.36	6.55	46.80	46.65	6.00
M-CN-N	12.52	1.97	0.39	7.83	42.91	49.27	6.95
D-CN-A	15.74	1.91	0.34	6.02	56.13	37.84	7.93
D-CN-N	16.96	2.23	0.48	10.90	64.84	24.27	10.16

<sup>a</sup> Average lifetime was calculated using equation:  $\tau_{av.} = (f_1\tau_1^2 + f_2\tau_2^2 + f_3\tau_3^2)/(f_1\tau_1 + f_2\tau_2 + f_3\tau_3)$ .

induced by the radiative/nonradiative recombination of photogenerated charge carriers, and thus, slower PL decay indicates longer charge carrier lifetime, which leads to a higher probability of charge involvement in photocatalytic reactions [56,57]. The result of time-resolved PL measurement suggests that CN materials generated in N<sub>2</sub> probably have higher catalytic activities than those generated in air. However, as mentioned in the conclusion, overall catalytic activity is determined by combination of various morphological and physical properties.

When the photocatalytic performances were measured, H<sub>2</sub>PtCl<sub>6</sub> was used to form Pt nanoparticles, as a co-catalyst, on g-C<sub>3</sub>N<sub>4</sub>. PtCl<sub>6</sub><sup>2-</sup> was reduced to Pt by photogenerated electrons from g-C<sub>3</sub>N<sub>4</sub>

[58]. TEM measurements of all six samples showed the generation of well-dispersed Pt particles (Fig. 8). The selected area electron diffraction (SAED) pattern shows diffraction spots from the crystalline Pt nanoparticles, corresponding to the (111), (200) and (220) reflections of face-centered cubic platinum (JCPDS: 04-0802) (Fig. S8) [59,60]. The energy dispersive spectroscopy (EDS) spectrum confirmed the presence of Pt, C, and N atoms from the sample (Fig. S9). It suggests that the Pt nanoparticles were successfully synthesized in the process of HER test. For U-CN-A, U-CN-N, M-CN-A, and D-CN-A samples, particle sizes were about 10–20 nm with narrow size distribution. Contrarily, M-CN-N and D-CN-N samples contain Pt particles with broader size distribution between 10 and 40 nm.

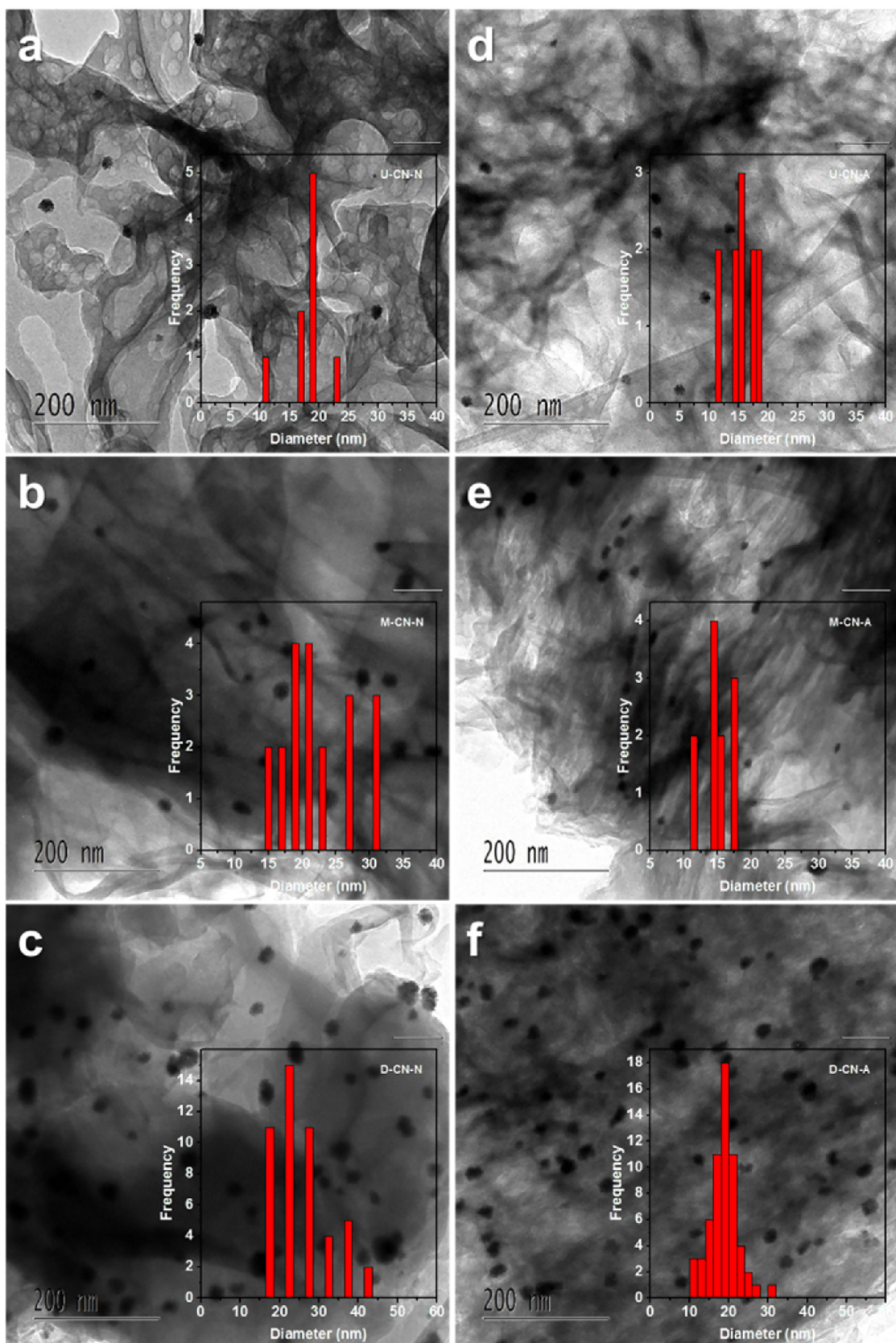


**Fig. 8.** TEM images of Pt nanoparticles on the  $\text{g-C}_3\text{N}_4$  samples and their particle size distribution (inlet) after 2 h visible light irradiation. a) U-CN-N, b) M-CN-N, c) D-CN-N, d) U-CN-A, e) M-CN-A, and f) D-CN-A.

As described above, the use of urea produced g-C<sub>3</sub>N<sub>4</sub> with higher surface area and more porosity regardless gas environments and air environment did it for melamine and dicyandiamide systems. Previous literatures reported that materials with higher surface area contain more numbers of growth sites for Pt particles, leading uniform distribution of small sized particles. It resulted in enhanced photocatalytic activities for HER [3,61].

When we compared the effects of precursors in same gas environments on the properties of the photocatalysts produced, they were found to be classifiable into two systems (melamine or dicyandiamide and urea systems). Band gaps of M-/D-CN samples were smaller than those of U-CN samples and the lifetimes of photogenerated charge carriers in D-CN samples were slightly longer than in U-CN samples (Table S5). As discussed above, a smaller band gap implies a better ability to use visible light and a longer lifetime a higher efficiency of electron injection to photocatalytic reactions. Consequently, we would expect that U-CN materials would show poorer catalytic activities than M-/D-CN materials, however, we found U-CN was the more efficient basis for HER. This apparent discrepancy could be explained by considerations of surface area in part. The significantly larger surface areas of U-CN materials give benefit to make them efficient catalysts and also to grow small-sized Pt nanoparticle co-catalysts with uniform size distribution. Additionally, as discussed above, *sp*<sup>3</sup> amine groups at the edges of C<sub>3</sub>N<sub>4</sub> networks can serve as active sites to initiate HER. Because of small grain size in U-CN, the larger number of amine groups provides another reason for its better catalytic performance.

Regarding the nature of gaseous environment, while the band gaps of M- and D-CN samples were identical to each other irrespective of whether they are produced in air or N<sub>2</sub>, the lifetime of photogenerated electrons was longer for M-CN-N/D-CN-N samples than for M-CN-A/D-CN-A samples. Although these observations suggest better catalytic performances for CN-N materials, based on the determined HER activities, the CN-A materials were found to have better catalytic performances. Once again, the surface area can explain this discrepancy. The surface areas of CN-A samples were greater than those of CN-N samples because, as mentioned above, the use of air leads to the generation of C<sub>3</sub>N<sub>4</sub> with a smaller grain size and a porous structure. As mentioned above, this morphological characteristic leads the growth of uniform- and small-sized Pt nanoparticles on the surface of g-C<sub>3</sub>N<sub>4</sub> during photodeposition process, which can increase the photocatalytic performances. Interestingly, when we calculated HER activities per surface area (Table 1), it was found that these normalized activities of CN-N samples were greater than those of CN-A samples, which indicates that the increase of surface area provides a means of generating efficient HER photocatalysts when melamine or dicyandiamide is used as a precursor. In this system, the difference of surface areas and N-(C)<sub>3</sub>/NH<sub>x</sub> ratios are bigger than that of bandgaps and lifetimes. It leads dominant effect of the former for the photocatalytic performances.

In the case of urea-based materials, the surface areas of U-CN-A and U-CN-N were almost identical, presumably because during the polycondensation of urea gas is generated due to the presence of O atoms in urea. In this case, surface area did not dictate catalytic performances and photophysical properties predominated. The smaller band gap of U-CN-N (2.78 eV) than of U-CN-A (2.86 eV) implied a better ability to utilize visible light. Additionally, the longer PL lifetime of U-CN-N increased the probability of transferring photogenerated electrons to support HER. In combination these factors appear to explain why the total and normalized photocatalytic activities of U-CN-N were better than those of U-CN-A. These results show that enhancing the photophysical properties of urea-based C<sub>3</sub>N<sub>4</sub> materials might be useful for producing more efficient HER photocatalysts.

## 4. Conclusions

Overall, we prepared six C<sub>3</sub>N<sub>4</sub> samples using three precursors (melamine, dicyandiamide, and urea) in two gas environments (air and N<sub>2</sub>) and investigated the photo-catalytic properties of the materials to identify the conditions required to generate efficient HER photocatalysts. Surface areas, porosity, grain sizes, band gaps, band positions, lifetimes of photogenerated charge carriers, and size distribution of Pt nanoparticles generated on the surface of g-C<sub>3</sub>N<sub>4</sub> were studied to understand materials' structure and properties.

The use of urea as a precursor and a N<sub>2</sub> environment produced the most efficient g-C<sub>3</sub>N<sub>4</sub> photocatalysts for hydrogen generation under visible light. It was found that under same gas environments, the use of urea as a precursor was beneficial to produce better photocatalysts than melamine and dicyandiamide. The photocatalytic activity was dominantly affected from surface area rather than light absorption ability. Materials with high surface area and porosity produced Pt nanoparticle co-catalysts with uniform size distribution on the surface of g-C<sub>3</sub>N<sub>4</sub>. Regarding the nature of gaseous environments, precursors can be classifiable into two systems (melamine/dicyandiamide and urea systems). In case of melamine and dicyandiamide systems, air condition produced materials with better catalytic performances than CN-N. In this case, the higher surface area with smaller grain size is a key factor for increasing the photocatalytic activity of g-C<sub>3</sub>N<sub>4</sub> materials. In a urea system, however, more efficient catalysts were produced under N<sub>2</sub> gas environment than air. While surface areas of the materials produced were almost identical regardless of gaseous environments, superior light absorption ability and photophysical properties became dominant factors to determine catalytic activity. The present study provides insight of the effect of synthetic conditions on the catalytic natures of the material produced.

## Acknowledgements

This work was supported by Inha University and grants from the Center for Advanced Soft Electronics as a Global Frontier Project (CASE-2013M3A6A5073173) and Basic Science Research Program (NRF-2015R1C1A1A02036958) through the National Research Foundation of Korea (NRF) funded by the Ministry of Science, ICT & Future Planning. S.P. thanks the Busan Center at the Korea Basic Science Institute (KBSI) for the XPS analysis.

## Appendix A. Supplementary data

Supplementary data associated with this article can be found, in the online version, at <http://dx.doi.org/10.1016/j.apcatb.2017.06.067>.

## References

- [1] A. Fujishima, Nature 238 (1972) 37–38.
- [2] X. Chen, S. Shen, L. Guo, S.S. Mao, Chem. Rev. 110 (2010) 6503–6570.
- [3] Y. Kang, Y. Yang, L. Yin, X. Kang, L. Wang, G. Liu, H. Cheng, Adv. Mater. 28 (2016) 6471–6477.
- [4] V.W. Lau, M.B. Mesch, V. Duppel, V. Blum, J. Senker, B.V. Lotsch, J. Am. Chem. Soc. 137 (2015) 1064–1072.
- [5] X. Kong, K. Xu, C. Zhang, J. Dai, S. Norooz Oliaee, L. Li, X. Zeng, C. Wu, Z. Peng, ACS Catal. 6 (2016) 1487–1492.
- [6] M.A. Lukowski, A.S. Daniel, F. Meng, A. Forticaux, L. Li, S. Jin, J. Am. Chem. Soc. 135 (2013) 10274–10277.
- [7] J. Xie, H. Zhang, S. Li, R. Wang, X. Sun, M. Zhou, J. Zhou, X.W.D. Lou, Y. Xie, Adv. Mater. 25 (2013) 5807–5813.
- [8] H. Li, C. Tsai, A.L. Koh, L. Cai, A.W. Contryman, A.H. Fragapane, J. Zhao, H.S. Han, H.C. Manoharan, F. Abild-Pedersen, Nat. Mater. 15 (2016) 48–53.
- [9] X. Kong, X. Shen, C. Zhang, S.N. Oliaee, Z. Peng, Inorg. Chem. Front. 3 (2016) 1376–1380.
- [10] H. Tang, K. Dou, C. Kaun, Q. Kuang, S. Yang, J. Mater. Chem. A 2 (2014) 360–364.

- [11] D. Voiry, H. Yamaguchi, J. Li, R. Silva, D.C. Alves, T. Fujita, M. Chen, T. Asefa, V.B. Shenoy, G. Eda, *Nat. Mater.* 12 (2013) 850–855.
- [12] X. Zhao, X. Ma, J. Sun, D. Li, X. Yang, *ACS Nano* 10 (2016) 2159–2166.
- [13] D. Kong, H. Wang, Z. Lu, Y. Cui, *J. Am. Chem. Soc.* 136 (2014) 4897–4900.
- [14] Y. Li, H. Wang, L. Xie, Y. Liang, G. Hong, H. Dai, *J. Am. Chem. Soc.* 133 (2011) 7296–7299.
- [15] H. Zhou, F. Yu, J. Sun, R. He, Y. Wang, C.F. Guo, F. Wang, Y. Lan, Z. Ren, S. Chen, *J. Mater. Chem. A* 4 (2016) 9472–9476.
- [16] C. Zhang, B. Wang, X. Shen, J. Liu, X. Kong, S.S. Chuang, D. Yang, A. Dong, Z. Peng, *Nano Energy* 30 (2016) 503–510.
- [17] Q. Li, B. Guo, J. Yu, J. Ran, B. Zhang, H. Yan, J.R. Gong, *J. Am. Chem. Soc.* 133 (2011) 10878–10884.
- [18] N. Bao, L. Shen, T. Takata, K. Domen, *Chem. Mater.* 20 (2007) 110–117.
- [19] A. Thomas, A. Fischer, F. Goettmann, M. Antonietti, J. Müller, R. Schlögl, J.M. Carlsson, *J. Mater. Chem.* 18 (2008) 4893–4908.
- [20] X. Wang, K. Maeda, A. Thomas, K. Takanabe, G. Xin, J.M. Carlsson, K. Domen, M. Antonietti, *Nat. Mater.* 8 (2009) 76–80.
- [21] J. Zhang, X. Chen, K. Takanabe, K. Maeda, K. Domen, J.D. Epping, X. Fu, M. Antonietti, X. Wang, *Angew. Chem. Int. Ed.* 49 (2010) 441–444.
- [22] Y. Kang, Y. Yang, L. Yin, X. Kang, G. Liu, H. Cheng, *Adv. Mater.* 27 (2015) 4572–4577.
- [23] J. Oh, R.J. Yoo, S.Y. Kim, Y.J. Lee, D.W. Kim, S. Park, *Chem. Eur. J.* 21 (2015) 6241–6246.
- [24] X. Zhang, X. Xie, H. Wang, J. Zhang, B. Pan, Y. Xie, *J. Am. Chem. Soc.* 135 (2012) 18–21.
- [25] J. Tian, Q. Liu, A.M. Asiri, A.O. Al-Youbi, X. Sun, *Anal. Chem.* 85 (2013) 5595–5599.
- [26] Z. Lin, X. Wang, *Angew. Ahem. Int. Ed.* 52 (2013) 1735–1738.
- [27] Z. Huang, J. Song, L. Pan, Z. Wang, X. Zhang, J. Zou, W. Mi, X. Zhang, L. Wang, *Nano Energy* 12 (2015) 646–656.
- [28] J. Hong, X. Xia, Y. Wang, R. Xu, *J. Mater. Chem.* 22 (2012) 15006–15012.
- [29] F. Goettmann, A. Fischer, M. Antonietti, A. Thomas, *Angew. Chem. Int. Ed.* 45 (2006) 4467–4471.
- [30] Y. Zhang, J. Liu, G. Wu, W. Chen, *Nanoscale* 4 (2012) 5300–5303.
- [31] F. Dong, Z. Wang, Y. Sun, W. Ho, H. Zhang, *J. Colloid Interface Sci.* 401 (2013) 70–79.
- [32] X. Song, Y. Hu, M. Zheng, C. Wei, *Appl. Catal. B* 182 (2016) 587–597.
- [33] D. Wang, J. Pan, H. Li, J. Liu, Y. Wang, L. Kang, J. Yao, *J. Mater. Chem. A* 4 (2016) 290–296.
- [34] W. Ong, L. Tan, S. Chai, S. Yong, *Chem. Commun.* 51 (2015) 858–861.
- [35] G. Zhang, J. Zhang, M. Zhang, X. Wang, *J. Mater. Chem.* 22 (2012) 8083–8091.
- [36] G. Zhang, X. Wang, *J. Catal.* 307 (2013) 246–253.
- [37] H. Yan, Y. Chen, S. Xu, *Int. J. Hydrogen Energy* 37 (2012) 125–133.
- [38] J. Zhang, J. Sun, K. Maeda, K. Domen, P. Liu, M. Antonietti, X. Fu, X. Wang, *Energy Environ. Sci.* 4 (2011) 675–678.
- [39] J. Zhang, G. Zhang, X. Chen, S. Lin, L. Möhlmann, G. Dołęga, G. Lipner, M. Antonietti, S. Blechert, X. Wang, *Angew. Chem.* 124 (2012) 3237–3241.
- [40] G. Zhang, M. Zhang, X. Ye, X. Qiu, S. Lin, X. Wang, *Adv. Mater.* 26 (2014) 805–809.
- [41] J. Liu, T. Zhang, Z. Wang, G. Dawson, W. Chen, *J. Mater. Chem.* 21 (2011) 14398–14401.
- [42] D.J. Martin, K. Qiu, S.A. Shevlin, A.D. Handoko, X. Chen, Z. Guo, J. Tang, *Angew. Chem. Int. Ed.* 53 (2014) 9240–9245.
- [43] Y. Yuan, W. Xu, L. Yin, S. Cao, Y. Liao, Y. Tng, C. Xue, *Int. J. Hydrogen Energy* 38 (2013) 13159–13163.
- [44] Z. Mo, X. She, Y. Li, L. Liu, L. Huang, Z. Chen, Q. Zhang, H. Xu, H. Li, *RSC Adv.* 5 (2015) 101552–101562.
- [45] Q. Gu, Z. Gao, H. Zhao, Z. Lou, Y. Liao, C. Xue, *RSC Adv.* 5 (2015) 49317–49325.
- [46] G. Dong, W. Ho, C. Wang, *J. Mater. Chem. A* 3 (2015) 23435–23441.
- [47] F. Dong, Y. Sun, L. Wu, M. Fu, Z. Wu, *Catal. Sci. Technol.* 2 (2012) 1332–1335.
- [48] Q. Tay, P. Kanhere, C.F. Ng, S. Chen, S. Chakraborty, A.C.H. Huan, T.C. Sum, R. Ahuja, Z. Chen, *Chem. Mater.* 27 (2015) 4930–4933.
- [49] M. Ciuéndez, M. Malmsten, J.C. Doadrio, M.T. Portolés, I. Izquierdo-Barba, M. Vallet-Regí, *J. Mater. Chem. B* 2 (2014) 49–58.
- [50] P.M. Schaber, J. Colson, S. Higgins, D. Thielen, B. Anspach, J. Brauer, *Thermochim. Acta* 424 (2004) 131–142.
- [51] T.A. White, S.E. Witt, Z. Li, K.R. Dunbar, C. Turro, *Inorg. Chem.* 54 (2015) 10042–10048.
- [52] A. Patterson, *Phys. Rev.* 56 (1939) 978.
- [53] J. Oh, Y.H. Chang, Y. Kim, S. Park, *Phys. Chem. Chem. Phys.* 18 (2016) 10882–10886.
- [54] E. Bundgaard, F.C. Krebs, *Sol. Energy Mater. Sol. Cells* 91 (2007) 954–985.
- [55] T. Wang, B. Daiber, J.M. Frost, S.A. Mann, E.C. Garnett, A. Walsh, B. Ehrler, *Energy Environ. Sci.* 10 (2017) 509–515.
- [56] P. Niu, L. Zhang, G. Liu, H. Cheng, *Adv. Funct. Mater.* 22 (2012) 4763–4770.
- [57] F. Dong, Z. Zhao, T. Xiong, Z. Ni, W. Zhang, Y. Sun, W. Ho, *ACS Appl. Mater. Interfaces* 5 (2013) 11392–11401.
- [58] T. Ohno, K. Sarukawa, M. Matsumura, *New J. Chem.* 26 (2002) 1167–1170.
- [59] M.F. Lengke, M.E. Fleet, G. Southam, *Langmuir* 22 (2006) 7318–7323.
- [60] S.J. Hoseini, M. Rashidi, M. Bahrami, *J. Mater. Chem.* 21 (2011) 16170–16176.
- [61] X. Li, W. Bi, L. Zhang, S. Tao, W. Chu, Q. Zhang, Y. Luo, C. Wu, Y. Xie, *Adv. Mater.* 28 (2016) 2427–2431.